Comparative study of multidisciplinary analysis of transonic strut-braced wing aircraft using different aerodynamic simulation fidelity levels

Shon Mori, Guillaume Arnoult, Mathieu Balesdent, Loïc Brevault, Cédric Liauzun, Sylvain Dubreuil

DOI: 10.13009/EUCASS2023-668
Aerospace Europe Conference 2023 – 10TH EUCASS – 9TH CEAS

Comparative study of multidisciplinary analysis of transonic strut-braced wing aircraft using different aerodynamic simulation fidelity levels

Shon Mori[⋆], *Guillaume Arnoult*[⋆], *Mathieu Balesdent*[†], *Loïc Brevault*[†], *Cédric Liauzun*[¶], *Sylvain Dubreuil*[§]
[⋆] *ONERA DAAA, Université Paris-Saclay*
F-92190, Meudon, France
shon.mori@onera.fr · guillaume.arnoult@onera.fr
[†] *ONERA DTIS, Université Paris-Saclay*
F-91123, Palaiseau, France
mathieu.balesdent@onera.fr · loic.brevault@onera.fr
[¶] *ONERA DTIS, Université Paris-Saclay*
F-92320 Châtillon, France
cedric.liauzun@onera.fr
[§] *ONERA DTIS, Université de Toulouse*
F-31055 Toulouse, France
sylvain.dubreuil@onera.fr

July 9, 2023

Abstract

This paper presents a comparative study of low and high-fidelity aero-structural Multi-Disciplinary Analysis (MDA) schemes for the High Aspect Ratio Strut-Braced Wing (HARSBW) concept. The vortex lattice method and compressible Euler aerodynamic solvers are utilized to construct the low and high-fidelity MDA schemes, respectively. The objective is to analyze the correlation between the two MDA fidelity and to evaluate the potential of constructing a multi-fidelity surrogate model for incorporation into Multi-Disciplinary Analysis and Optimization (MDAO) architecture. The MDA runs are performed for varying Mach numbers and Angle of Attack (AoA) values. The results indicate that the different level fidelity MDA schemes approximately correlate with a wide range of AoA values and lower Mach conditions. However, at higher Mach numbers (Mach number > 0.68), potential discordance between the two fidelity-level MDA schemes is observed. These findings provide valuable insights for developing efficient global MDAO architectures, particularly for the preliminary aircraft design of HARSBW concept.

1. Introduction

1.1 Research context

Reducing the environmental impact of the civil aviation industry is a pressing challenge that requires addressing various aspects of aircraft design and operations. While incremental improvements have been made in components such as propulsion systems, materials, and fuels,[1] the conventional fuselage and cantilever wing design have remained largely unchanged for decades. To achieve further efficiency gains, it is necessary to explore disruptive and innovative configurations beyond the traditional design.

Among the potential design candidates, the High Aspect Ratio Strut-Braced Wing (HARSBW) concept shows promise.[2] Evaluating the feasibility and optimal performance of this unconventional configuration requires conducting Multi-Disciplinary Analysis and Optimization (MDAO).[3] This process involves conducting Multi-Disciplinary Analysis (MDA) for various potential design configurations to explore the design space and thoroughly analyze the corresponding aero-structural behavior, which is of key importance in the HARSBW concept. The MDA couples the aerodynamic and the structural simulation to iteratively find the fluid-structure static equilibrium state.[2] The iterative nature of the MDA exacerbates the computational expense of high-fidelity Computational Fluid Dynamics (CFD) solvers based on compressible Euler or Navier-Stokes equations.[4] Thus, within the context of the MDA process, the use of low-fidelity

DOI: 10.13009/EUCASS2023-668

solvers with less computational cost is of great interest. These include solvers based on Vortex Lattice Method (VLM) and the panel method with potential flow formulations.[5]

In order to establish an efficient and accurate MDAO scheme, the use of a multi-fidelity approach may be able to provide the necessary solver resolution whilst maintaining a low computational budget.[6] This methodology requires the fusion of the results from different fidelity-level solvers in various methodologies and thus depends on the approximate agreement of these results.[7] This study is aimed to investigate the potential utilization of the MDA based on different aerodynamic solver fidelities in the multi-fidelity MDAO scheme applied to the HARSBW design by comparing its respective responses.

1.2 Research problem and objective

The primary constraint in exploring the design space during the preliminary aircraft design process is its large dimensionality. One of the major limiting factors in conducting a full MDAO process within this vast design space is the problem of the computational cost of disciplinary solvers in the MDA process, especially the high-fidelity fluid dynamics solvers required for accurate modeling of aircraft airflow. This study entails a comparative analysis of the MDA conducted for a chosen HARSBW configuration based on low and high-fidelity aerodynamic solvers. VLM and compressible Euler CFD solver was chosen as the low and high-fidelity aerodynamic solvers, respectively. Two independent MDA schemes are presented, each associated with the fidelity level of the incorporated aerodynamic solver. The results of the MDA schemes are compared to each other based on the series of MDA conducted for two variables, Mach number and angle of attack of the flight condition. The objective outcome of this study is to identify the potential points of compatibility and discordance between the two fidelity-level MDA schemes. The results of this analysis are aimed at serving the construction of multi-fidelity MDAO schemes for the preliminary aircraft design of HARSBW.

1.3 Overview

This paper first introduces some background information on the major components of the aero-structural MDA and its application case, the HARSBW concept, in Section 2. Later, in Section 3, the details of the constructed low and high-fidelity aerodynamic model and structural model generation chain are described. Furthermore, the integration of these models in the low and high-fidelity MDA schemes is presented. Finally, in Section 4, the results from a series of MDA runs with varying flight conditions are presented. The convergence iterations, converged geometries, and their associated aerodynamic coefficients from these trials are compared between the two MDA schemes.

2. Literature Review

2.1 Strut-braced wing concept and its design challenges

The strut-braced wing concept, HARSBW, and its variants, known as the truss-braced wing concept, have gained increasing interest recently due to their potential for performance improvement.[8] In the HARSBW concept, the wing is supported by a strut member connected to the fuselage, allowing for a higher aspect ratio while reducing the bending moment at the wing root through structural support. Achieving the same aspect ratio as the traditional aircraft designs will require significantly increased structural weight to support the extended wing span, as the cantilever wing design relies on structural support provided solely by the wing root. The increase in the wing aspect ratio reduces induced drag and promotes laminar flow, resulting in the reduction of drag.[2] Pfenninger initially proposed the concept in the 1950s as a transonic aircraft configuration.[9] Since the 2000s, it has been further studied as an MDAO application.[10–14] Currently, the concept is being researched by institutions such as the UHARWARD project under the CleanSky2 European Commission program,[2] Transonic Truss-Braced Wing project by NASA and The Boeing Company[15] and the Gullhyver concept developed by ONERA.

Existing studies highlight the particular complexity of the HARSBW concept in the MDA context due to the intricate coupling of aerodynamic and structural phenomena resulting from its high aspect ratio wings and its junction between the strut and wing.[16] The structural analysis must consider aeroelastic phenomena like flutter,[13] limit loading cases, and strut buckling.[17] The intended transonic flight regime further complicates the aerodynamic analysis as higher fidelity solvers, such as Euler or Reynolds Averaged Navier-Stokes (RANS), are required to capture the compressibility effects. The flow interaction at the wing-strut juncture, functioning analogously to a nozzle, accelerates the flow locally, and creates shocks.[18] The HARSBW model utilized in this study avoids strong shock formation by incorporating a vertical strut section at the junction between the wing and the strut, as well as fairings at the wing and strut with the fuselage. These complexities make the HARSBW concept a challenging case for developing multi-fidelity MDAO

DOI: 10.13009/EUCASS2023-668

for preliminary aircraft design, as it may highlight the potential incompatibilities in MDA based on different fidelity aerodynamic models.

2.2 MDA architecture

To evaluate preliminary aircraft design performance, Fluid-Structure Interaction (FSI) analysis must be conducted by coupling the aerodynamic and structural disciplines in the MDA as shown in Figure 1 and Equation 1 to find the converged aircraft geometry under flight loads.[4] The superscripts a and s indicate the association with the aerodynamic or structural solver, respectively. The aerodynamic solver $\mathcal{M}^a$ produces the aerodynamic forces, denoted as $\boldsymbol{f}^a$, at each node of the relevant aircraft component surface mesh. Similarly, the structural solver $\mathcal{M}^s$ provides the structural displacement, represented as $\boldsymbol{u}^s$, at each node of the corresponding aircraft component structural mesh. To incorporate the aerodynamic forces $\boldsymbol{f}^a$ as input in the structural solver, it is necessary to transfer these forces onto the structural mesh, resulting in $\boldsymbol{f}^s$. Likewise, the structural solver's output, $\boldsymbol{u}^s$, must be projected onto the aerodynamic surface mesh to obtain $\boldsymbol{u}^a$, ensuring the generality of the proposed method.

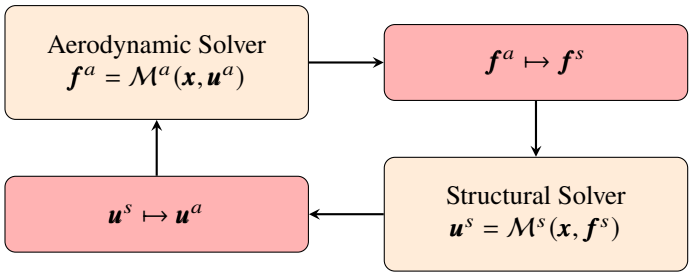

Figure 1: Aero-structural MDA with field coupling variables

$$\begin{cases} \boldsymbol{f}^a = \mathcal{M}^a(\boldsymbol{x}, \boldsymbol{u}^a) \\ \boldsymbol{u}^s = \mathcal{M}^s(\boldsymbol{x}, \boldsymbol{f}^s) \end{cases} \tag{1}$$

Exploring the entire design space with numerous variables and online simulations for each discipline compounds the computational cost. One of the potential methodologies to incorporate the multi-fidelity approach to this process is using surrogate models based on discipline-specific data, trained with calls to low and high-fidelity solvers, to reduce the need for costly solver calls during design space exploration.[19] This will allow for the multi-fidelity surrogate model based MDA to capture the various aerodynamic phenomena only able to be perceived by the high-fidelity solvers, whilst enabling extensive design space exploration due to the reduced computational cost of the low-fidelity solvers. However, this relies on the approximate accordance of the MDA responses based on the low and high-fidelity aerodynamic solvers. The point of comparison for the compatibility of the different fidelity level MDA schemes is the common mesh field outcomes, as this will allow us to adopt strategies to build multi-fidelity surrogate models by constructing the snap-shots on this MDA outcomes.[19] In the context of this study, the structural model mesh serves as a common mesh between the two fidelity-level aerodynamic model based MDA. Therefore the correlation of the converged MDA geometry forms will give an indication of the compatibility of the two fidelity-level MDA.

2.3 Aerodynamic solvers

The low-fidelity aerodynamic solver chosen for this study is Athena Vortex Lattice (AVL).[20] AVL is an open-source software tool used for aerodynamics analysis. It employs the vortex lattice method, a simplified computational fluid dynamics model, to calculate aerodynamic forces and moments acting on an aircraft. The method represents lifting surfaces and their wakes as interconnected horseshoe vortex filaments organized in a grid of single-layer vortex sheets. By solving the governing equations using the Biot-Savart Law and Kutta-Joukovsky theorem,[21] VLM solvers can determine lift and pressure distributions, induced drag, and pitching moments experienced by the aircraft. However, AVL, like other analytical aerodynamic models, has certain limitations. It assumes an incompressible, inviscid, and irrotational flow field, and uses small angle estimations for the angle of attack (AoA). Consequently, it neglects unsteady vorticity shedding and exhibits limited accuracy in simulating highly compressible flows. AVL incorporates the 3D Prandtl-Glauert transformation to reliably model quasi-steady subsonic compressible flow up to a perpendicular flow Mach number of 0.6. However, its simulations become less reliable beyond this point, particularly when the flow becomes transonic over the model. Therefore, when dealing with transonic flight conditions, relying solely on AVL or similar low-fidelity solvers using the panel method poses challenges in obtaining reliable results within the context of

DOI: 10.13009/EUCASS2023-668

MDA. In the case of the HARSBW concept, which shares a similar service profile with the Airbus Industrie A321 LR cruising at Mach number 0.78, AVL results need to be complemented by data from higher-fidelity solvers. Additionally, VLM only computes induced drag due to the potential flow formulation, necessitating the use of higher-fidelity solvers or their post-processing capabilities to calculate profile and wave drag for a more comprehensive analysis.

The high-fidelity solver chosen for this study must accurately simulate steady-state compressible flow regimes, capture profile, and wave drag, and maintain computational efficiency. The compressible Euler equations enable the computation of compressible flow simulations by modeling inviscid, adiabatic, and irrotational fluid motion. The open-source multi-physics simulation software suite SU2[22] provides a versatile platform based on the finite volume method, which discretizes the governing equations on a computational mesh. SU2's compatibility with the unstructured mesh method fits the intended application case; it accommodates the automated meshing of parametrically generated aircraft models, which is vital in the larger context of MDAO. Furthermore, using the Euler method limits the time consumption of the mesh generation process compared to RANS or other higher-fidelity computations requiring mesh refinement at the geometry surface to capture boundary layer interactions. SU2 also includes built-in mesh deformation capabilities crucial for the MDA process. However, the computational cost of the compressible Euler equation CFD poses a limitation in the context of MDAO, which is addressed by utilizing AVL as the low-fidelity counterpart. Additionally, the far-field drag (FFD) post-processing analysis tool developed by ONERA provides the drag breakdown (wave and induced drag) based on the far-field approach.[23]

3. Methodology

The parametric definition of the HARSBW concept has been defined.[24] The generation of the structural and aerodynamic models for this study is based on a set of chosen design parameters based on this parametric definition. This ensures a consistent geometric representation between the solvers. The model generation process, as well as the pre and post-processing procedure required for each solver, are detailed in its respective sections below.

3.1 Low-fidelity aerodynamic model

VLM model in AVL is represented by vertical and horizontal planes, which are discretized into horseshoe vortex elements. The geometrical definition utilizes the symmetry between the left and right-hand sides of the plane. The geometry is delineated by setting the leading edge of the geometry in the cross-section and then specifying the chord at the given section for the surface. An airfoil can be assigned at this defined chord to effectively change the camber by using the airfoil mean camber line. The fuselage and other non-lifting aircraft elements can be modeled with slender body element type.

In order to model the deformation of the wings, the defined plane is subdivided into 25 discretizations on the semi-span. This allows for the curvature of the deformed wing to be represented by moving these definitions in a coherent manner. The strut deformation is modeled as a straight element whilst keeping the same attachment point at the fuselage and wing. Meanwhile, the fuselage and tail planes are modeled as static. The generation and deformation of the AVL model geometry are done through developed Python programs. The visualization of the model and the results within the AVL software is limited and thus requires extensive post-processing to obtain the necessary results. Figure 3 exhibits the undeformed model simulation at Mach number of 0.65 and AoA of 2.5°. The geometry visualization from the AVL environment is shown on the left, and the post-processed vertical aerodynamic force vector visualization is shown on the right.

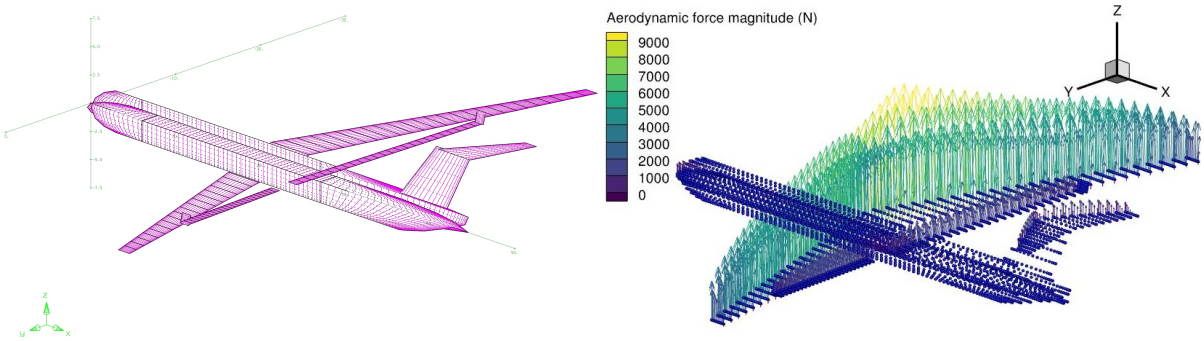

(a) Visualization in AVL interface

(b) Post-processed vortex wise aerodynamic force

Figure 2: Undeformed AVL simulation at Mach = 0.65 and AoA = 2.5°

DOI: 10.13009/EUCASS2023-668

3.2 High-fidelity aerodynamic model

The process of generating a parametric model for SU2 is synchronized with AVL and NASTRAN to ensure geometric consistency among the three solvers. The automated model generation and meshing procedure for SU2 computation involve several main steps. Firstly, Engineering Sketch Pad (ESP)[25] and Engineering Geometry Aircraft Design System (EGADS)[26] are utilized to generate the geometry based on the specified top-level design parameters. These tools enable the creation of accurate geometric representations that align with the desired design parameters. Subsequently, Computational Aircraft Prototype Syntheses (CAPS)[27] takes advantage of the interconnected Analysis Interface Modules (AIM)[28] to pre-process the generated geometry for the SU2 computation run. CAPS acts as a bridge between the geometric model and the subsequent analysis steps, facilitating data transfer and preparation.

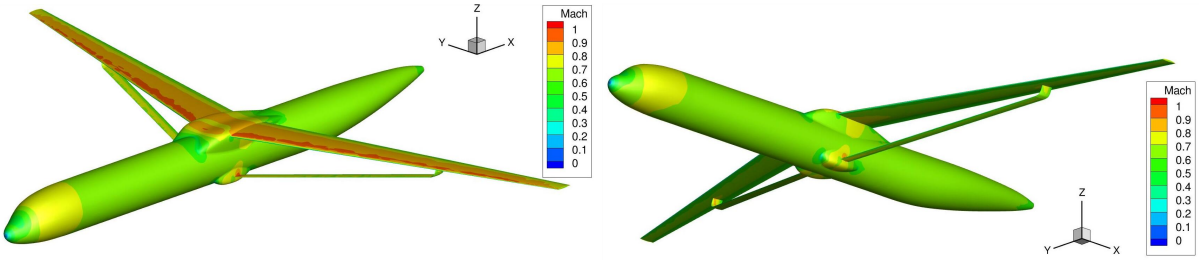

(a) Surface flow Mach - bottom view

(b) Surface flow Mach - top view

Figure 3: Undeformed SU2 simulation at Mach number= 0.65 and AoA = 2.5°

One of the AIM modules employed in this process is Pointwise,[29] a commercial meshing software. Pointwise is responsible for automatically generating the Euler mesh, which consists of approximately 4 million cells, for the generated aircraft model. Following the mesh generation, the SU2 module within AIM enables the execution of the SU2 solver, which performs compressible Euler simulations. For post-processing, the FFD module calculates the various drag components, including wave drag, viscous drag, and induced drag. These components contribute to the overall drag generated by the aircraft and provide valuable insights into its aerodynamic performance. In summary, the process of automated model generation and meshing for SU2 computation involves synchronized interactions between ESP, EGADS, CAPS, Pointwise, and the SU2 solver. This integrated approach ensures the accuracy and consistency of the geometric representation and allows for comprehensive aerodynamic analysis.

3.3 Structural model

In this study, the structural finite element method (FEM) solver NASTRAN[30] fulfills the role of generating the flexibility matrix, a condensed static model of the FEM model that captures the structural response generated by the NASTRAN calculation chain. The linear FEM model consists of beam elements with six degrees of freedom, translation, and rotation in the three-dimensional axis. However, in the broader context of holistic parametric preliminary aircraft design optimization, the structural discipline must also possess the capability to size the internal structural members (thickness of ribs, stringers, and skin members) to withstand the different loading cases according to the parametrically generated external geometry. In this study, the internal structure has been sized using the parametric NASTRAN model, which sizes the internal structure based on the geometry dictated by the same design parameters utilized for the SU2 and AVL models. The structure is sized under limited loading conditions: 2.5g pull-up maneuver, -1g taxi bump, and cruise under a safety factor of 2.0 whilst minimizing weight. Flutter analysis is also conducted additionally to this optimization and structural sizing process using SOL145 to ensure it does not occur in the set flight envelope. Figure 4 exhibits the generated structural model for this case.

Figure 4 shows the detailed representation of the internal structures within the wing, dictating its deformation characteristics. For the HARSBW concept, this primarily includes the long and narrow wings, which undergo significant deformation, particularly influenced by the strut acting as a structural support member. In the model, the strut is represented as a single beam member constrained in tension to prevent buckling. The flexibility matrix enables efficient calculation of structural deformation in response to applied forces and moments at defined force application nodes. Figure 5 shows the nodes at which the aerodynamic forces are applied (blue) and the displacement nodes (blue and red) where the flexibility matrix outputs its displacement and rotation. The procedure with which the aerodynamic forces and moments are applied for the two MDAs is detailed in Section 3.4.

DOI: 10.13009/EUCASS2023-668

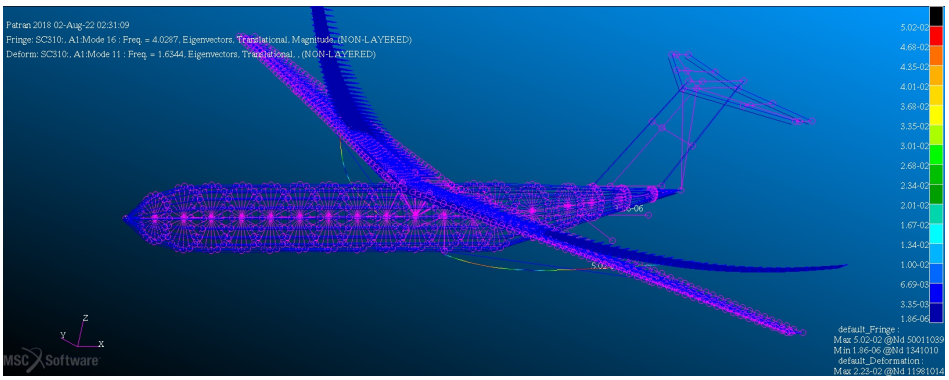

Figure 4: Structural model of HARSBW

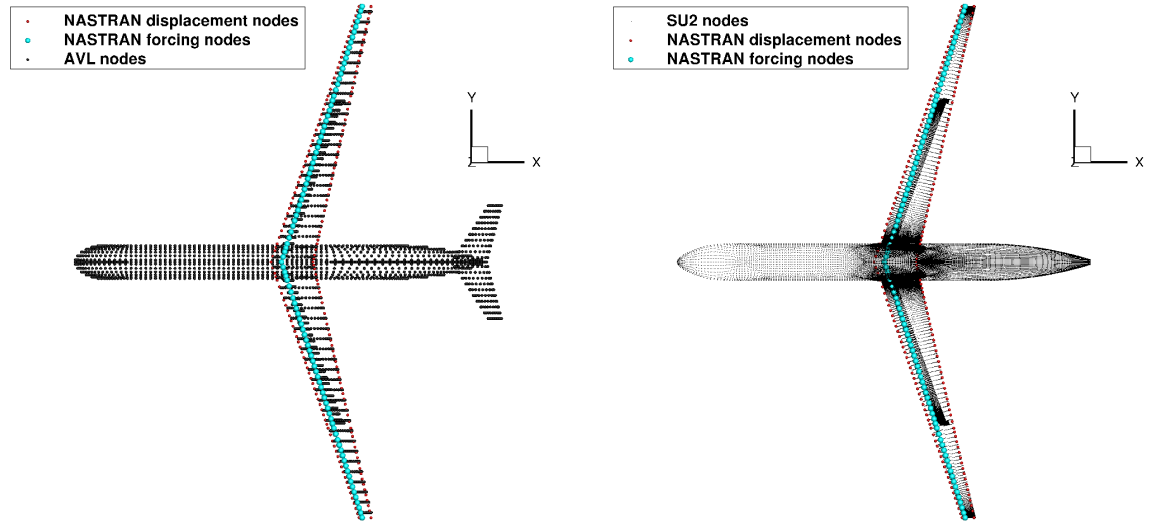

(a) Low-fidelity aerodynamics and structural model nodes - XY view (b) High-fidelity aerodynamics and structural model nodes - XY view

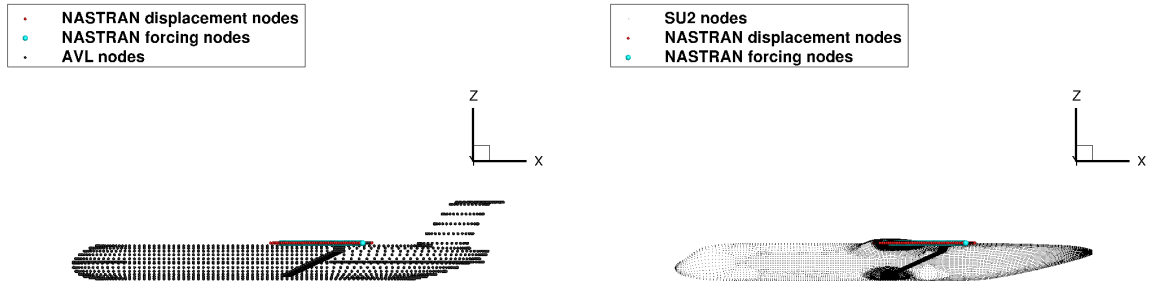

(c) Low-fidelity aerodynamics and structural model nodes - XZ view (d) High-fidelity aerodynamics and structural model nodes - XZ view

Figure 5: Low and high-fidelity aerodynamic and structural model nodes

3.4 MDA scheme

By utilizing the aforementioned aerodynamic model generation and deformation tools developed in conjunction with the structural calculation chain, the low and high-fidelity MDA schemes are constructed. The outline of the constructed MDA scheme is presented in Figure 6, where it details the high-fidelity MDA scheme. Some key differences exist in the MDA procedure between the low and high-fidelity MDA schemes, including the SU2 model generation chain presented in the *Model Generation* block in red is handled by the aforementioned AVL model generation tool for the low-fidelity MDA. However, the NASTRAN model generation and outputted flexibility matrix, $\mathcal{F}$, is identical to that incorporated in the high-fidelity MDA scheme.

The web application tool for MDAO, WhatsOpt,[31] is utilized to construct the MDA framework for both high and

DOI: 10.13009/EUCASS2023-668

low-fidelity MDA schemes. WhatsOpt allows users to construct complex MDAO schemes via the online graphical user interface and output OpenMDAO[32] scripts with inbuilt input and output control between the disciplinary solvers to establish the coupling between the disciplines. Similar to the scheme presented in Figure 6, WhatsOpt scripts handle the aerodynamic simulation configuration inputs: AoA, Mach number, and updated deformed mesh during the MDA iterations. The aerodynamic simulation is shown in the first green process in the low-fidelity MDA is done by AVL. The major difference in running the aerodynamic simulations between the two MDA is in how the SU2 computation is submitted to the HPC to be computed with 48 Broadwell cores. The SU2 computation is conducted with 30 iterations for each MDA iteration, and by using the restart flow for each nonlinear block Gauss-Seidel (fixed point) solver iteration of the MDA, the SU2 simulations are converged collectively. Meanwhile, for the low-fidelity MDA scheme, AVL simulations are computed on a single core of Intel® Xeon® CPU E5-2650 v4 2.20GHz. The result is post-processed to obtain the discredited vortex horseshoe aerodynamic forces for AVL and surface mesh node-wise aerodynamic forces for SU2, $\boldsymbol{f}^a$.

The transfer of $\boldsymbol{f}^a$ onto the structural forcing nodes, shown in blue and red nodes in Figure 5 is accomplished using the k nearest neighbor (k-NN) algorithm.[33] This process isolates the wings from the rest of the model and allocates the closest structural node for each aerodynamic node. With the vector that forms between these nodes, the force and the moment resulting from $\boldsymbol{f}^a$ can be summed onto the structural nodes to obtain $\boldsymbol{f}^s$. These associations and their respective vectors are used to reverse the process of applying the computed structural node displacements using the flexibility matrix, $\boldsymbol{u}^s$, to the aerodynamic nodes for AVL to obtain $\boldsymbol{u}^a$. The strut geometry is modeled as a straight beam, maintaining the same connection point at the fuselage and the wing surface.

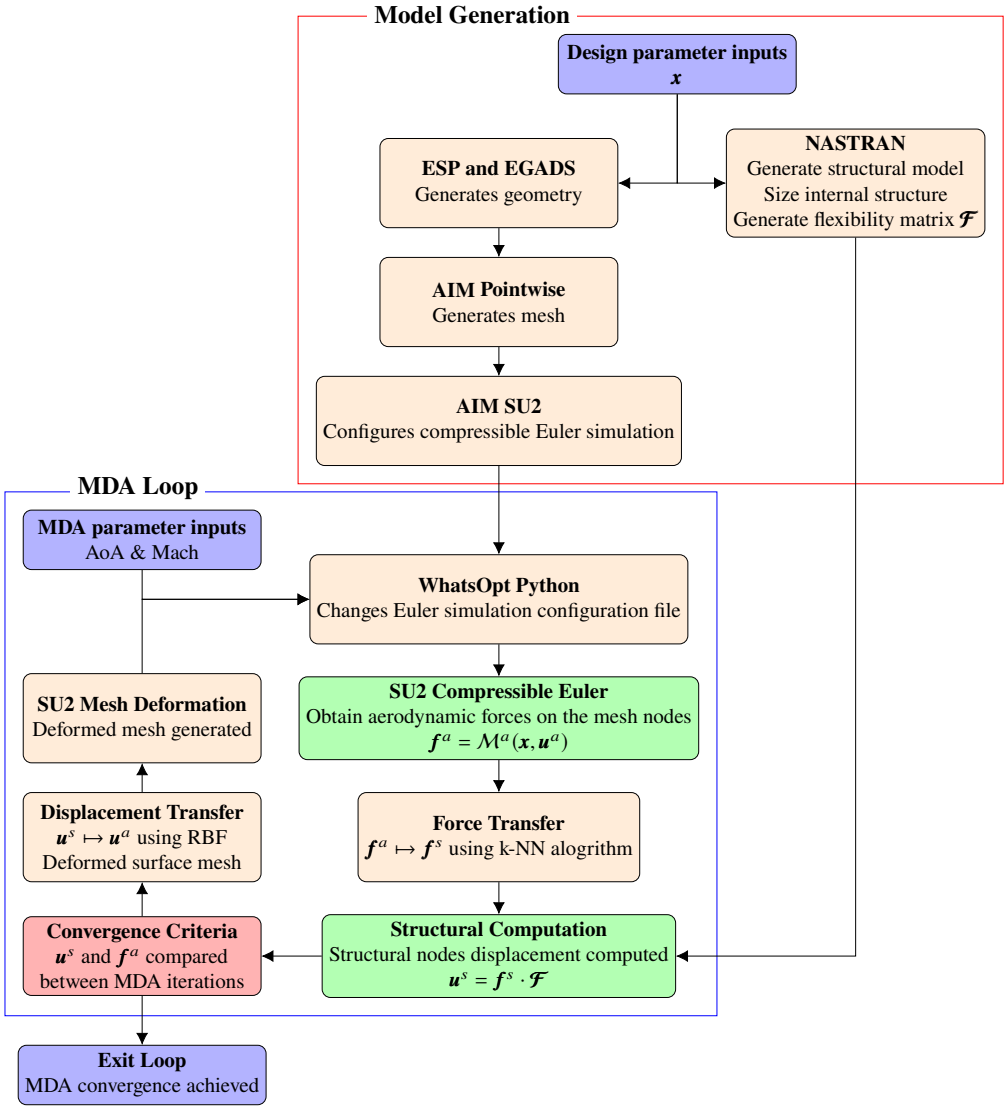

Figure 6: SU2 model generation and MDA architecture

This process, shown in Figure 6 as *Displacement Transfer*, is different for the high-fidelity MDA, where Radial

DOI: 10.13009/EUCASS2023-668

Basis Function (RBF)[34] is utilized to interpolate the displacement of the structural nodes depending on their X-Y (aircraft fixed horizontal plane) position, using the thin plate spline kernel. Additional dummy structural nodes are added in the RBF interpolation process along the center axis of the fuselage with zero displacements and rotation to avoid the RBF interpolation deforming components other than the wing and strut. Furthermore, the forces and moments, as well as the displacement and rotation applied to and obtained from the structural nodes in the section overlapping the fuselage and wing-fuselage fairings, are set to zero to model the aerodynamic and structural behavior at this junction. The interpolated displacements are computed for the surface nodes of the entire aircraft model to obtain $\boldsymbol{u}^a$. This ensures a smooth deformation of the mesh without discontinuities and thus avoids issues with CFD simulation convergence.

For the low-fidelity model, the deformed model is constructed by analyzing the deformed locations of the vortex nodes and by fitting the geometry definition and vortex lattice discretizations to match these distributions. This involves using the deformed vortex nodes to calculate the local dihedral angle and the angle of incidence for each span-wise segment of the wing, as well as its quarter chord location and its chord length. By constructing the AVL model definition for each wing segment to match this geometrical information, the deformed wing can be constructed in AVL. For the high-fidelity MDA, the deformation of the Euler mesh is conducted by the mesh deformation functionality in-built in SU2. This program deforms the mesh according to the inputted deformed surface mesh of the model.

The convergence of the MDA using a nonlinear block Gauss-Seidel algorithm is monitored with the relative error of the norm of the vector of the structural displacement $\boldsymbol{u}^s$ and aerodynamic force $\boldsymbol{f}^a$ between the iterations. As elements of $\boldsymbol{u}^s$ tend to zero and $\boldsymbol{f}^a$ to constant values through this non-linear Gauss-Seidel iterations, the geometry oscillates about the equilibrium state as shown in Figures 7 and 8. For this study, the relative error criteria for convergence is set to 0.01. Thus, the difference between the aforementioned criteria values must be below 1% between the iterations. The convergence of the two MDA schemes as well as the aerodynamic coefficients and geometries of the converged models are compared to analyze the compatibility of the schemes in the construction of a multi-fidelity surrogate model to be utilized in the global MDAO of the preliminary design of the HARSBW concept. The MDA loop is run for a varying AoA between 0.0° and 5.0° in increments of 0.5° whilst keeping the same Mach number of 0.65, to see the effect of AoA on the MDA process. Furthermore, the MDA loop was run for varying Mach number between 0.5 and 0.74 in increments of 0.03 at constant AoA of 2.5°, to investigate the effect of Mach number on the MDA process.

4. Results and Discussion

The results of the varying AoA and Mach number MDA runs, as detailed in Section 3.4 are presented in this section. The convergence performance of the MDA schemes is in Section 4.1. The converged geometries from the different MDA run conditions are examined in Section 4.2. Furthermore, the converged geometry and its aerodynamic coefficients are compared between the MDAs for the range of test conditions in Section 4.3. Throughout the analysis of the results, its implications for the construction of a multi-fidelity surrogate model are discussed.

4.1 MDA convergence

The intermediary states of the MDA iterations are visualized in Figure 7 for the low-fidelity MDA and Figure 8 for the high-fidelity MDA. The oscillations of the non-linear Gauss-Seidel iterations can be observed as it converges to the equilibrium state. The oscillations are larger in the low-fidelity MDA compared to the high-fidelity MDA. Consequently, this results in increased number of MDA iterations required to converge to the equilibrium state, as shown in Table 1. Note that relaxation methods such as Aitken relaxations, normally used for aero-structural MDA applications,[35] are omitted to observe the MDA performances in a more direct manner.

For the comparison of the computation times, as presented in Table 1, the entire scheme for both low and high-fidelity MDA was run on a single core of Intel® Xeon® CPU E5-2650 v4 2.20GHz for the varying AoA MDA runs. Although the high-fidelity MDA can be accelerated by running the CFD computation on HPC cores, this comparison exhibits the computational cost of the high-fidelity MDA. This result shows the advantage of incorporating low-fidelity aerodynamic solvers in constructing multi-fidelity MDAO architecture as a means to lower the computational cost. The varying Mach number with constant AoA MDA runs has exhibited an increased number of iterations for the increasing Mach number, as shown in Figure 9. This was not observed for the constant Mach number, varying AoA MDA runs, which maintained a near-constant number of iterations required for the MDA convergence.

The increasing number of iterations due to the increase in Mach number impacts both low and high-fidelity MDA as shown by Figure 9. Thus, this will not impact the viability of constructing a multi-fidelity surrogate model for the global MDAO process using the two fidelity levels. This result warrants further investigation into the layout of the high-fidelity solver calls in the MDA, as a higher number of CFD computation iterations can be set for the first MDA iteration to allow for convergence of the CFD simulation earlier in the process to reduce the overall number of MDA iterations necessary.

DOI: 10.13009/EUCASS2023-668

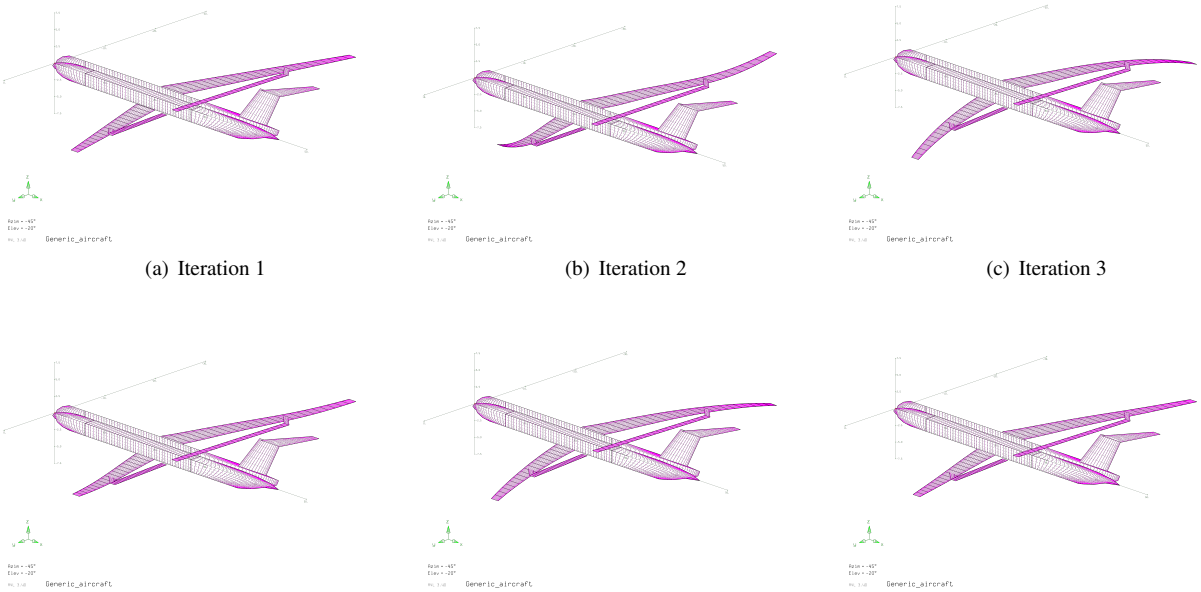

(a) Iteration 1 (b) Iteration 2 (c) Iteration 3

(d) Iteration 4 (e) Iteration 5 (f) Iteration 6

Figure 7: AVL model geometry for the first six iterations of MDA at Mach number = 0.65 and AoA = 2.5°

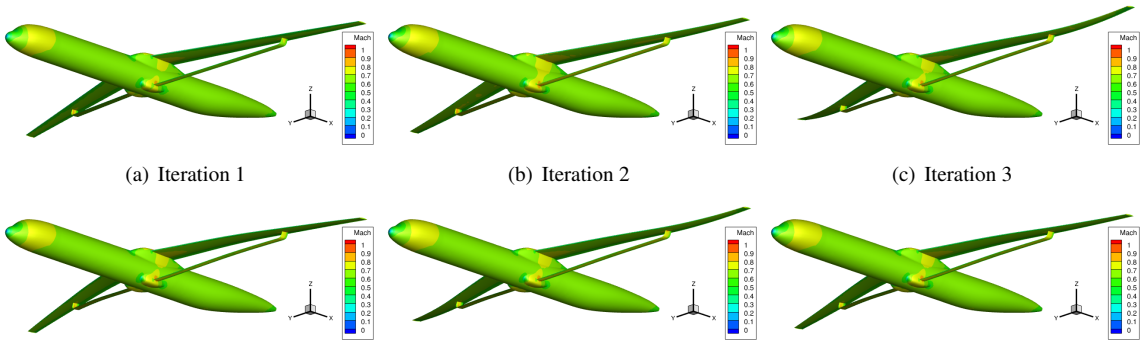

(a) Iteration 1 (b) Iteration 2 (c) Iteration 3

(d) Iteration 4 (e) Iteration 5 (f) Iteration 6

Figure 8: SU2 model geometry for the first six iterations of MDA at Mach number = 0.65 and AoA = 2.5°

Table 1: MDA convergence performance

	Mean no. of iterations	**Mean time (sec/iteration)**	**Mean total time (sec)**
Low-fidelity MDA	14	68.0	952.0
High-fidelity MDA	8.82	425.0	3748.5

The performance of the low and high-fidelity MDA schemes exhibit clear viability for the construction of multi-fidelity MDAO schemes due to the difference in the computational costs. Furthermore, the potential for applying different CFD computation integration strategies within the MDA process was observed.

4.2 Converged Geometry

The converged geometries can be compared between the low and high-fidelity MDA schemes to serve as an indicator of the similarity of the aerodynamic force distribution obtained for the converged MDA model. This is useful for the analysis of the viability of the construction of the multi-fidelity surrogate model for the aerodynamic discipline as it will be constructed on the aerodynamic solver's output response transferred onto the common mesh between the two disciplines. Thus, this is the aerodynamic forces transferred onto the structural nodes using the k-NN algorithm $\boldsymbol{f}^s$.

Figures 10 and 11 exhibit the converged geometry for the MDA runs at AoA of 0.0°, 2.5° and 5.0°, at fixed Mach number of 0.65. The red nodes show the AVL model vortex horseshoe discretizations and the blue surface shows

DOI: 10.13009/EUCASS2023-668

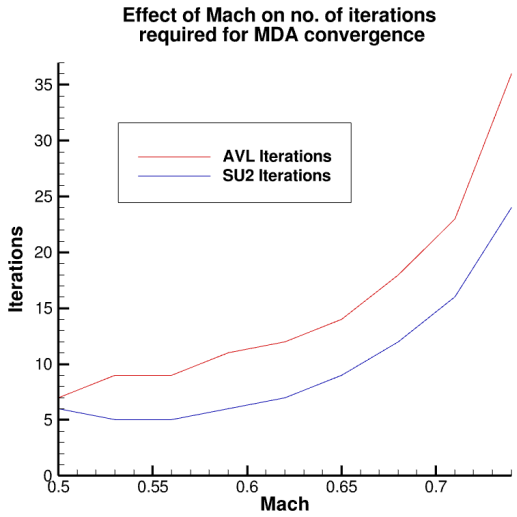

Figure 9: Impact of Mach number on the number of iterations required for MDA convergence

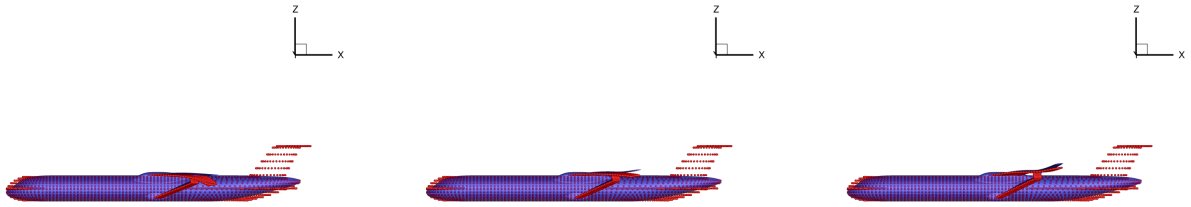

(a) Mach number = 0.65 and AoA = 0.0° (b) Mach number = 0.65 and AoA = 2.5° (c) Mach number = 0.65 and AoA = 5.0°

Figure 10: Converged AVL (red nodes) and SU2 (blue surface) MDA geometry with varying AoA - XZ view

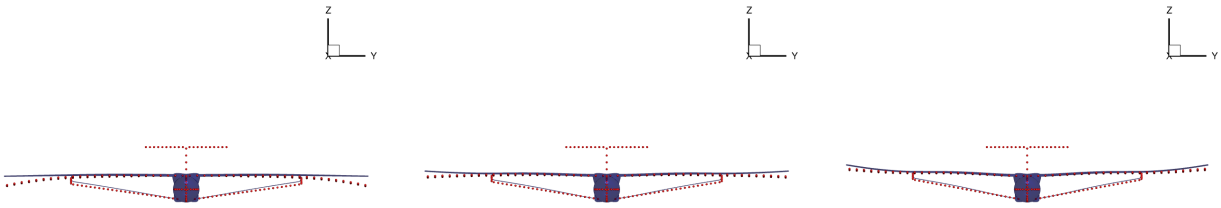

(a) Mach number = 0.65 and AoA = 0.0° (b) Mach number = 0.65 and AoA = 2.5° (c) Mach number = 0.65 and AoA = 5.0°

Figure 11: Converged AVL (red nodes) and SU2 (blue surface) MDA geometry with varying AoA - YZ view

the SU2 model geometry. The deformed geometry aligns well at the higher AoA, and the difference between the two models can be observed for the other AoA runs. However, the general trend of the converged model deformation can be observed to align. The wing tips have a negative angle twist angle for lower AoA due to the attachment of the strut and the aerodynamic forces resulting in a downward twisting moment. This creates a downward lift at the wingtips, resulting in a downturned wing curvature along its span from the wing-strut joint to the wing tip.

With an increased AoA, this moment is reversed, creating an upward twisting moment and thus increased lift upwards at the wingtips. This phenomenon appears for lower AoA values in the SU2 model, probably due to the difference in chord-wise lift force distribution between the two solvers, as shown in Figure 12. This figure shows the elevated lift force generated at the trailing edge in AVL for low AoA conditions, in comparison to the SU2 computations. However, the cross-sectional surface pressure coefficient shown in Figure 12(c) indicates a similar pressure distribution and the existence of the negative lift production at the wing tips observed in the AVL model but at lower magnitudes in comparison to AVL results. This further supports the alignment of the trends captured between the two-fidelity level MDA schemes. Furthermore, this phenomenon of twisting wing tips due to the strut support in relation to lift distribution is unique to the HARSBW concept and shows that it is captured both in the low and high-fidelity MDA schemes. The construction of the multi-fidelity surrogate model will depend on the correlation of the trends captured

DOI: 10.13009/EUCASS2023-668

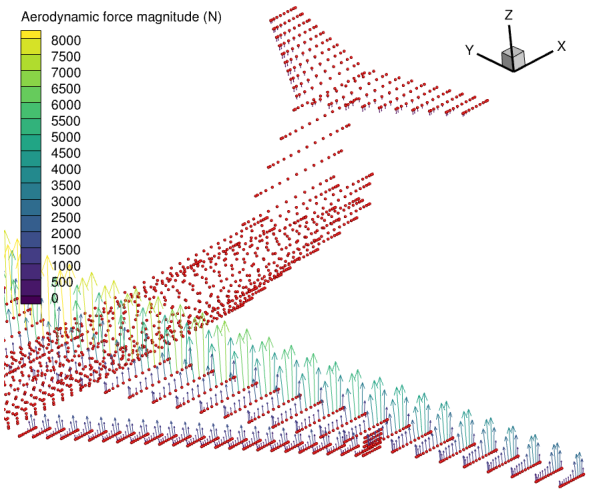

(a) AVL aerodynamic force distribution

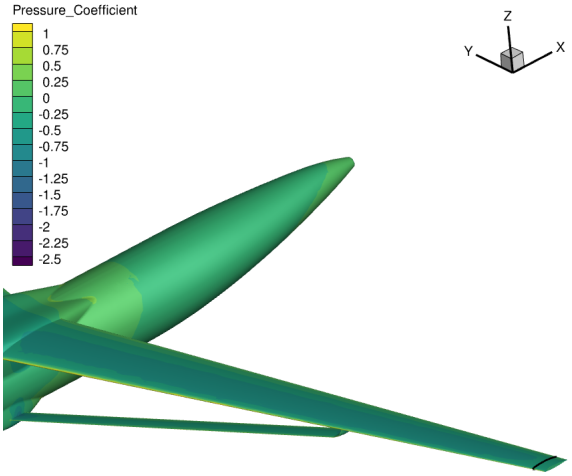

(b) SU2 pressure coefficient distribution with cross-section location indication

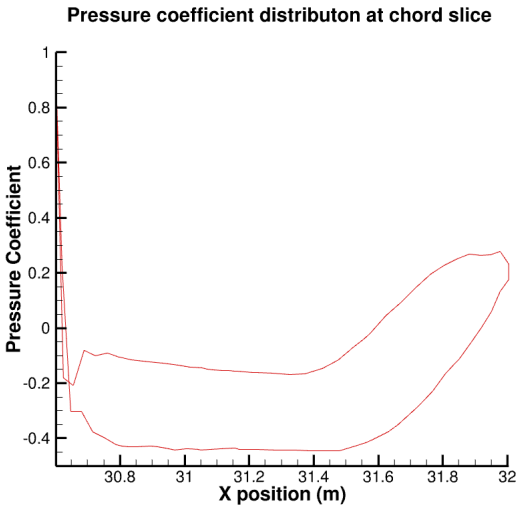

(c) Pressure coefficient distribution along the wing surface at the wing tip cross-section indicated with black line on 12(b)

Figure 12: Distribution of aerodynamic efforts for undeformed model at Mach number = 0.65 and AoA = 0.0°

by the nodal output of the two aerodynamic solvers. Thus, this result further supports the compatibility of the two solvers in this application.

Figures 13 and 14 show the converged geometry for the MDA runs at Mach number of 0.5, 0.65, and 0.74 at fixed AoA of 2.5°. Whilst additional MDA was run for Mach number of 0.77 and 0.80 for both schemes, AVL showed

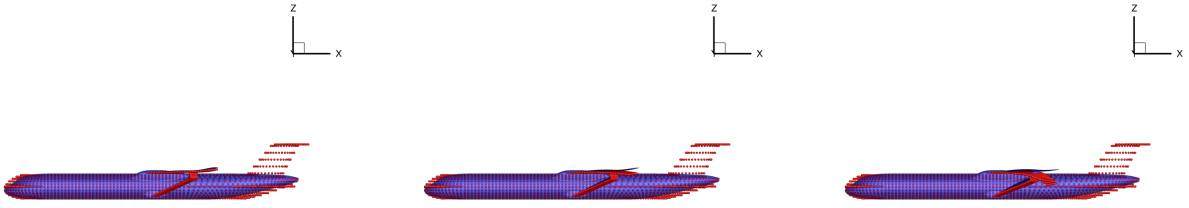

(a) Mach number = 0.50 and AoA = 2.5° (b) Mach number = 0.65and AoA = 2.5° (c) Mach number = 0.74 and AoA = 2.5°

Figure 13: Converged AVL (red nodes) and SU2 (blue surface) MDA geometry with varying Mach number - XZ view

DOI: 10.13009/EUCASS2023-668

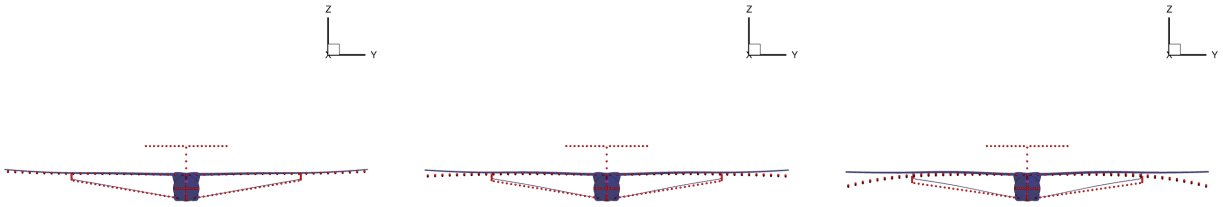

(a) Mach number = 0.50 and AoA = 2.5° (b) Mach number = 0.65 and AoA = 2.5° (c) Mach number = 0.74 and AoA = 2.5°

Figure 14: Converged AVL (red nodes) and SU2 (blue surface) MDA geometry with varying Mach number - YZ view

completely unrealistic aerodynamic coefficient results for its converged geometry, and the SU2 Euler computations diverged during its extended MDA iterations. This highlights the limitations of both MDA schemes that need to be addressed to explore the design space completely in the intended MDAO process. With lower Mach numbers, the two MDA schemes exhibited good alignment of the converged geometry. However, the alignment diverges with higher Mach numbers. This may be due to the limitation of AVL as a vortex lattice method solver to model compressible flows. More investigation is warranted for this divergent trend in other AoA runs. It can be hypothesized, based on the results observed in Figures 10 and 11, that with higher AoA, the varying Mach number MDA runs will show better alignment. However, this is a potential point of incompatibility for using AVL as the low-fidelity aerodynamic solver in higher Mach conditions.

4.3 Aerodynamic coefficients

The aerodynamic coefficients result from the converged MDA geometry aerodynamic simulations are exhibited in Figure 15. The output of the aerodynamic coefficients for AVL is limited to the coefficient of lift (CL) and coefficient of induced drag (CDi). The FFD analysis incorporated in the high-fidelity MDA iterations can output a comprehensive breakdown of the aerodynamic coefficients.

The dotted lines are AVL results, and the solid lines are SU2 Euler results, whilst the red lines indicate the CL and the blue lines signify the CDi. The results from the varying AoA MDA runs are shown on the graph on the left. Both CL and CDi trends are in good alignment, indicating the compatibility of the solvers in constructing a multi-fidelity MDAO scheme. However, for the varying Mach number MDA runs, the results show a limited correlation of trends for the CL and divergence for CDi. These results further support the observations made in Section 4.2, where the higher Mach conditions lead to a worsened correlation of the trends between the low and high-fidelity MDA schemes. The rapid decrease in CL and increase in CDi for the AVL result at higher Mach conditions are reflected in the differences seen in the converged geometries observed in Figure 14(c). Although the aerodynamic coefficients are not directly

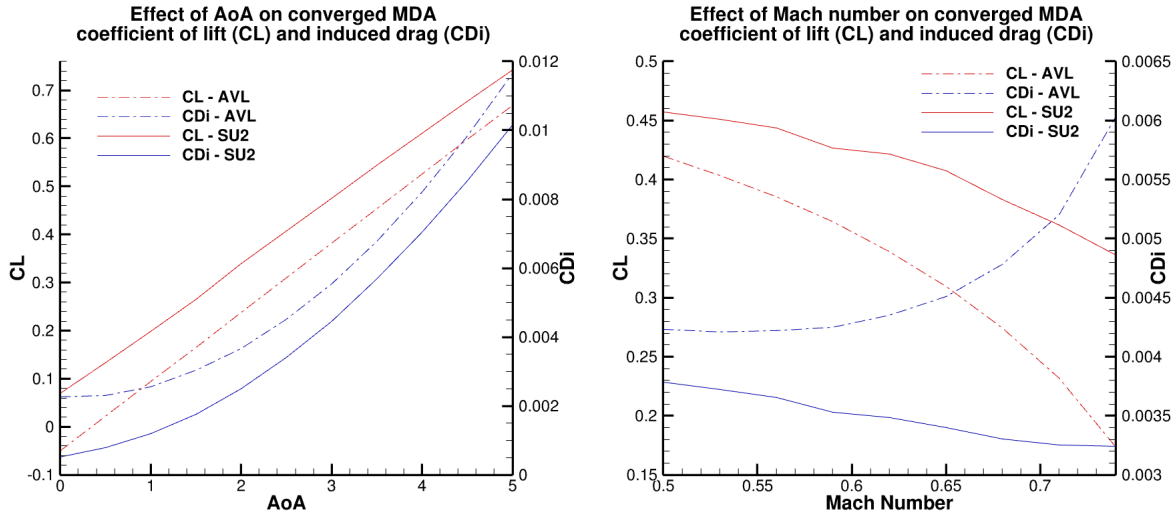

(a) AoA dependent CL and CDi (b) Mach number dependent CL and CDi

Figure 15: Impact of AoA and Mach number on the converged MDA lift and induce drag coefficient

DOI: 10.13009/EUCASS2023-668

utilized for constructing a multi-fidelity surrogate model, this result gives an insight into the reasoning for whether the converged geometries from the two MDAs are correlating well or not.

5. Conclusion

The low and high-fidelity Multi-Disciplinary Analysis (MDA) schemes have been constructed using AVL and SU2 Euler CFD solvers, respectively, for the High Aspect Ratio Strut-Braced Wing (HARSBW) concept. The comparison of the MDA schemes is necessary to identify the potential aspects of compatibility and incompatibility between the two fidelity-level aerodynamic solvers to construct a multi-fidelity surrogate model of the nodal output of the disciplinary solvers. This is intended to construct efficient global Multi-Disciplinary Analysis and Optimization (MDAO) MDAO architecture. A series of MDA runs have been conducted for two variables, Mach number and Angle of Attack (AoA). The results showed that the multi-fidelity MDAO scheme utilizing a combination of low and high-fidelity aerodynamic solvers may be compatible with a range of varying AoA and lower Mach conditions. The study also identified the potential discordance between the two fidelity-level MDA schemes at higher Mach conditions (Mach number > 0.68). The results of the analysis can serve as a basis for constructing multi-fidelity MDAO schemes for the preliminary aircraft design of HARSBW.

6. Acknowledgments

This study was funded by the European Union under the CleanSky2 joint undertaking as part of the AIRFRAME ITD NACOR project.

References

[1] Martin Sohst, José Lobo do Vale, Frederico Afonso, and Afzal Suleman. Optimization and comparison of strut-braced and high aspect ratio wing aircraft configurations including flutter analysis with geometric non-linearities. *Aerospace Science and Technology*, 124:107531, 2022.

[2] Gerald G Carrier, Guillaume Arnoult, Nicolo Fabbiane, Jean-Sebastien Schotte, Christophe David, Sébastien Defoort, Emmanuel Benard, and Martin Delavenne. Multidisciplinary analysis and design of strut-braced wing concept for medium range aircraft. In *AIAA SCITECH 2022 Forum*, page 0726, 2022.

[3] Wrik Mallik, Rakesh K Kapania, and Joseph A Schetz. Multidisciplinary design optimization of medium-range transonic truss-braced wing aircraft with flutter constraint. *AIAA/ASME/ASCE/AHS/ASC Structures, Structural Dynamics, and Materials Conference*, 54, April 2013.

[4] Peter Nagy, Bryn Jones, Edmondo Minisci, Marco Fossati, Alvaro Cea, Rafael Palacios, Nicolas Roussouly, and Anne Gazaix. Multi-fidelity nonlinear aeroelastic analysis of a strut-braced ultra-high aspect ratio wing configuration. In *AIAA AVIATION 2022 Forum*, page 3668, 2022.

[5] Tahura Shahid, Faiza Sajjad, Muneeb Ahsan, Syed Farhan, Shuaib Salamat, and Messam Abbas. Comparison of flow-solvers: Linear vortex lattice method and higher-order panel method with analytical and wind tunnel data. In *2020 3rd International Conference on Computing, Mathematics and Engineering Technologies (iCoMET)*, pages 1–7, 2020.

[6] Sylvain Dubreuil, Nathalie Bartoli, Christian Gogu, and Thierry Lefebvre. Towards an efficient global multidisciplinary design optimization algorithm. *Structural and Multidisciplinary Optimization*, 62:1739–1765, 2020.

[7] Loïc Brevault, Mathieu Balesdent, and Ali Hebbal. Overview of gaussian process based multi-fidelity techniques with variable relationship between fidelities, application to aerospace systems. *Aerospace Science and Technology*, 107:106339, 2020.

[8] Ohad Gur, Joseph A Schetz, and William H Mason. Aerodynamic considerations in the design of truss-braced-wing aircraft. *Journal of Aircraft*, 48(3):919–939, 2011.

[9] Werner Pfenninger. Special course on concepts for drag reduction. laminar flow control. lamina-rization. *AGARD Rep*, (654), 1977.

DOI: 10.13009/EUCASS2023-668

[10] Joel M Grasmeyer, A Naghshineh, PA Tetrault, B Grossman, RT Haftka, RK Kapania, WH Mason, and JA Schetz. Multidisciplinary design optimization of a strut-braced wing aircraft with tip-mounted engines. *MAD Center Report MAD*, pages 98–01, 1998.

[11] John Gundlac, Philippe-Andre Tetrault, Frank Gern, Amir Nagshineh-Pour, Andy Ko, Joseph Schetz, William Mason, Rakesh Kapania, Bernard Grossman, and Raphael Haftka. Multidisciplinary design optimization of a strut-braced wing transonic transport. *Aerospace Sciences Meeting Exhibit*, 38, January 2000.

[12] Frank H Gern, Andy Ko, Erwin Sulaeman, John F Gundlach, Rakesh K Kapania, and Raphael T Haftka. Multidisciplinary design optimization of a transonic commercial transport with strut-braced wing. *Journal of Aircraft*, 38(6), November 2001.

[13] Ohad Gur, Manav Bhatia, Joseph A Schetz, William H Mason, Rakesh K Kapania, and Dimitri N Mavris. Design optimization of a truss-braced-wing transonic transport aircraft. *Journal of Aircraft*, 47(6), November 2010.

[14] Yoann Le Lamer, Joseph Morlier, Emmanuel Benard, and Ping He. Aeroelastic analysis of high aspect ratio and strut-braced wings. In *33th Congress of the International Council of the Aeronautical Sciences*, page 11 p., Stockholm, Sweden, September 2022.

[15] Nhan T Nguyen, Juntao Xiong, and Jason Fugate. Multi-point jig twist optimization of mach 0.745 transonic truss-braced wing aircraft and high-fidelity cfd validation. In *AIAA Scitech 2021 Forum*, page 0338, 2021.

[16] Rauno Cavallaro and Luciano Demasi. Challenges, ideas, and innovations of joined-wing configurations: a concept from the past, an opportunity for the future. *Progress in Aerospace Sciences*, 87:1–93, 2016.

[17] Andy Ko, Bernard Grossman, W Mason, and R Haftka. The role of constraints in the mdo of a cantilever and strut-braced wing transonic commercial transport aircraft. In *2000 World Aviation Conference*, page 5609, 2000.

[18] Andy Ko, William Mason, and Bernard Grossman. Transonic aerodynamics of a wing/pylon/strut juncture. *Applied Aerodynamics Conference*, 21, June 2003.

[19] Gaspard Berthelin, Sylvain Dubreuil, Michel Salaün, Nathalie Bartoli, and Christian Gogu. Disciplinary proper orthogonal decomposition and interpolation for the resolution of parameterized multidisciplinary analysis. *International Journal for Numerical Methods in Engineering*, 123(15):3594–3626, 2022.

[20] Mark Drela and Harold Youngren. Athena vortex lattice. *Software Package, Ver*, 3, 2004.

[21] John Anderson. *EBOOK: Fundamentals of Aerodynamics (SI units)*. McGraw hill, 2011.

[22] Thomas D Economon, Francisco Palacios, Sean R Copeland, Trent W Lukaczyk, and Juan J Alonso. Su2: An open-source suite for multiphysics simulation and design. *AIAA Journal*, 54(3):828–846, 2016.

[23] Michaël Méheut and Didier Bailly. Drag-breakdown methods from wake measurements. *AIAA Journal*, 46(4):847–862, 2008.

[24] Gerald Carrier, Olivier Atinault, Sylvie Dequand, Jean Luc Hantrais-Gervois, Cédric Liauzun, Bernard Paluch, Anne Marie Rodde, and Clement Toussaint. Investigation of a strut-braced wing configuration for future commercial transport. pages 2012–1, 2012.

[25] Robert Haimes and John Dannenhoffer. The engineering sketch pad: A solid-modeling, feature-based, web-enabled system for building parametric geometry. In *21st AIAA Computational Fluid Dynamics Conference*, page 3073, 2013.

[26] John E Melton. Egads: A microcomputer program for estimating the aerodynamic performance of general aviation aircraft. Technical report, 1994.

[27] Robert Haimes, Marshall C Galbraith, John F Dannenhoffer III, David L Marcum, and Steve Karman. Computational aircraft prototype synthesis (caps). Technical report, Massachusetts Institute of Technology, 2019.

[28] Robert Haimes, John Dannenhoffer, Nitin D Bhagat, and Darcy L Allison. Multi-fidelity geometry-centric multi-disciplinary analysis for design. In *AIAA Modeling and Simulation Technologies Conference*, page 4007, 2016.

[29] Cadence Design Systems, Inc. Fidelity pointwise, 2022.

DOI: 10.13009/EUCASS2023-668

[30] RH MacNeal and CW McCormick. The nastran computer program for structural analysis. *Computers & Structures*, 1(3):389–412, 1971.

[31] Rémi Lafage, Sebastien Defoort, and Thierry Lefebvre. Whatsopt: a web application for multidisciplinary design analysis and optimization. In *AIAA Aviation 2019 Forum*, page 2990, 2019.

[32] Justin S Gray, John T Hwang, Joaquim RRA Martins, Kenneth T Moore, and Bret A Naylor. Openmdao: An open-source framework for multidisciplinary design, analysis, and optimization. *Structural and Multidisciplinary Optimization*, 59:1075–1104, 2019.

[33] Evelyn Fix and Joseph Lawson Hodges. Discriminatory analysis. nonparametric discrimination: Consistency properties. *International Statistical Review/Revue Internationale de Statistique*, 57(3):238–247, 1989.

[34] Thomas CS Rendall and Christian B Allen. Unified fluid–structure interpolation and mesh motion using radial basis functions. *International journal for numerical methods in engineering*, 74(10):1519–1559, 2008.

[35] Gaetan KW Kenway, Graeme J Kennedy, and Joaquim RRA Martins. Scalable parallel approach for high-fidelity steady-state aeroelastic analysis and adjoint derivative computations. *AIAA journal*, 52(5):935–951, 2014.